Crystallization pathways and some properties of lithium disilicate oxynitride glasses

S.P. Singh, A.M. Rodrigues, H.D. Orsolini, P.P.G. De Mattos, E.D. Zanotto, J. Rocherullé, Patricia Benard-Rocherulle, Ronan Lebullenger

Crystallization pathways and some properties of lithium disilicate oxynitride glasses

Shiv Prakash Singh[a,*], Alisson Mendes Rodrigues[a], Heloisa Daltoso Orsolini[a], Paulo Parreira Gomes de Mattos[a], Edgar Dutra Zanotto[a,*], Jean Rocherullé[b], Patricia Bénard-Rocherullé[b], Ronan Lebullenger[b]

[a]*Vitreous Materials Laboratory (LaMaV), Department of Materials Engineering, Federal University of São Carlos, São Carlos-SP, Brazil*

[b]*Glass and Ceramic Laboratory, Chemical Sciences Institute (UMR CNRS 6226), University of Rennes 1, France*

ABSTRACT

Lithium silicates have been used as model glasses for scientific and technological studies of glass-ceramics because they easily crystallize in the interiors, even without the addition of any nucleating agent. On the other hand, partial replacement of oxygens with nitrogens affects most properties of oxide glasses, but its effect on the crystallization kinetics of the glasses has been poorly documented. In this work, we report, for the first time, on the crystallization kinetics of nitrited lithium silicate glasses. The oxynitride glasses were prepared by partial substitution of oxygen by nitrogen, up to 6 at.% N/(N+O), by melt-quenching the liquid under N_2 atmosphere inside a glove box. As expected, the density, microhardness, and Young's modulus of the glasses improved with increasing nitrogen content. Higher values of glass transition and crystallization peak temperatures were also obtained with an increase in the nitrogen content. Rietveld refinement analysis after adequate thermal treatment revealed that addition of nitrogen led to increasingly higher contents of lithium metasilicate at the expense of the (expected) lithium disilicate crystal phase. Crystallization kinetic parameters such as the activation energy and

Avrami index were calculated using Ozawa's equations. These two parameters also increased with increasing nitrogen content, whereas the crystal growth rates decreased with increasing nitrogen content. The above-described changes in the properties of the oxynitride glasses are straightforwardly explained by the increase in the connectivity of the glass network, which results in enhancement of the atomic packing density owing to partial substitution of two-coordinated oxygens by three-coordinated nitrogens.

*Co-corresponding authors.

Email addresses: dedz@ufscar.br (E.D. Zanotto), spsingh67@gmail.com (S.P. Singh)

1. Introduction

The discovery of glass-ceramics by S. D. Stookey in the early 1950s fostered extensive research work on the interrelations among their composition, processing, crystallization kinetics, and the resulting microstructures, properties, and potential applications [1-4]. In this context, lithium disilicate ($Li_2Si_2O_5$) glasses have been extensively used for investigating the crystallization kinetics and thermal, mechanical, and electrical properties of the resulting glass-ceramics [5-9]. Lithium-disilicate-based glass-ceramics have commercial significance and have been widely used in dental restoration, armor material, hard disc substrates, and other high-tech applications owing to their good processability and mechanical performance [10-14].

Stoichiometric lithium disilicate glass is a relatively good glass-former that undergoes internal (homogeneous) crystallization when properly heated, even without the addition of any nucleating agents. This glass can exhibit two stages: amorphous and fully crystalline [15-18]. Therefore, the properties of lithium disilicate glass-ceramics can be tuned within a wide range through adjustment of the relative amounts of the glass and crystal phases as well as of the crystal size. Overall, the lithium disilicate system has been extensively studied in terms of its nucleation and growth kinetics [17,19-22].

In view of the above background, introduction of nitrogen into this glass composition could be an interesting strategy to not only improve some properties but also understand its effect on the crystallization kinetics. Studies over the last decades have shown that addition of nitrogen to oxide glasses significantly affects their physical, chemical, mechanical, optical, and thermal properties [23-27]; however, information on the crystallization kinetics and on oxynitride glass-ceramics is scarce. For instance, the glass transition and crystallization temperatures, the elastic moduli, and the lithium mobility increase [28] whereas the thermal

expansion coefficient decreases [29-30]. Introduction of nitrogen into stoichiometric $Li_2Si_2O_5$ glass through partial substitution of two-coordinated oxygen atoms by three-coordinated nitrogen atoms is probably a key reason for the change in properties, because it results in a glass structure with a greater degree of connectivity [25, 26, 30]. This increase in the degree of network connectivity, along with the more covalent nature of the Si-N bonding, causes the glass network to contract and rigidify. Several studies have been conducted on oxynitride glasses, and some of the most relevant ones are discussed below.

Luo *et al.* [31] prepared La-Ca-Al-Si-O-N oxynitride glasses and investigated the effects of N/O and La/Ca ratios (equiv%) on the density, thermal expansion coefficient, glass transition temperature, crystallization temperature, Vickers hardness, bending strength, and leaching rate. They found that nitrogen enhances the beneficial effects of lanthanum on all of these properties. Luo *et al.* [32] also prepared Zn-Sr-Y-sialon glasses by melting batches under N_2 atmosphere. They conducted an infrared spectroscopy study to determine the structural units of these glasses. They evaluated the relative ballistic resistance (D_{rel}) by using some physical and mechanical properties. They found that D_{rel} of a particular oxynitride glass sample $Y_{12}Zn_9Sr_3Al_{20}Si_{56}O_{82}N_{18}$ (equiv%) was 2.65 which is higher than that of sapphire and anticipated that oxynitride glasses are promising transparent armor materials.

Sauze *et al.* [33] prepared phosphorus oxynitride glasses with compositions of $15R_2O$-$15K_2O$-$15R'O$-$5Al_2O_3$-$50P_2O_5$ and $12R_2O$-$12K_2O$-$20R'O$-$6Al_2O_3$-$50P_2O_5$ mol% (R = Li or Na; R′ = Mg, Ba, or Zn), which were exposed to ammonia above 600°C for up to several days. They found that nitrogen increases the glass transition temperature and decreases the thermal expansion coefficient and the dissolution rate in water. These changes in the properties of phosphorus oxynitride glasses resulted from the strengthening of the glass network by

substitution of P-N for P-O bonds. Paraschiv *et al.* [34] studied the influence of nitridation of metaphosphate glasses on the liquid fragility by means of calorimetric measurements. They found that incorporation of nitrogen into the phosphate network led to a strengthened, polymerized network. Hence, this phenomenon contributed to higher T_g and densities and to lower liquid fragility.

In an another study, Qu *et al.* [35] prepared M-Si-Al-O-N (M = Y, Ca, or Mg) oxynitride glasses by melting batches at 1600°C for 2 h under N_2 atmosphere. They studied the crystallization behavior and microstructure of glasses containing different modifiers. The results revealed that the thermal treatment had a significant influence on the volume fraction of the crystalline phases and on the resulting microstructure of the glass-ceramics, as expected, but it had a small effect on the types of precipitated crystalline phases. For the 24Y18N glass composition, no crystals precipitated under two heat treatment conditions (900°C/2 h + 1150°C/2 h and 900°C/2 h + 1150°C/4 h). However, when the heat treatment duration was extended to 6 h, formation of mullite ($Al_6Si_2O_{13}$) was observed. In the 24Ca18N glass-ceramic, two crystal phases, gehlenite ($Ca_2Al_2SiO_7$) and anorthite ($CaAl_2Si_2O_8$) were identified. The $(Mg,Al)SiO_3$, $Mg_2(SiO_4)$, and $MgAl_2O_4$ phases crystallized in the 24Mg18N glass-ceramic after adequate heat treatment. The authors reported that it is more difficult to precipitate crystals from the 24Y18N glass composition than from the 24Ca18N and 24Mg18N glass compositions. They observed that these crystal phases did not include any nitrogen-containing crystal phases, which resulted in an increase in the nitrogen content of the residual glass in comparison to that of the parent glass. Their results agreed with those of a former study on Mg-Y-Si-A1-O-N glasses [36]. An oxide glass heat-treated at 1373 K for 10 h showed α-cordierite $Mg_2Al_4Si_5O_{18}$ as the main crystalline phase and spinel $Y_{4.67}Si_3O_{13}$ as the secondary phase. The diffraction pattern of an oxynitride

glass subjected to a similar heat treatment at 1423 K for 10 h showed the presence of only magnesium spinel $MgAl_2O_4$. As a consequence, the residual glassy phase was enriched in nitrogen, and this resulted in an increase in the viscosity and the activation energy for crystallization.

Rocherullé and coworkers conducted nonisothermal devitrification studies on LiSiAlON glasses, in which the Li/Si atomic ratio was the same as that in N-free lithium disilicate [37-38]. They found that both the oxide glass and the oxynitride glass had the same crystalline phases (Li_2SiO_3 and $Li_{0.6}Al_{0.6}Si_{2.4}O_6$). No evidence of the presence of nitrogen was found in the crystals, but the overall activation energy for crystallization and the Avrami index increased in the case of the oxynitride glass.

To the best of our knowledge, no study has thus far been conducted to examine the mechanism and crystallization kinetics of oxynitride lithium disilicate glass-ceramics, which is a highly important model glass-ceramic for many scientific studies and technological applications. Therefore, the aim of the present study is to investigate the effects of partial substitution of oxygen by nitrogen on the crystallization of lithium disilicate glass.

2. Experimental procedures

2.1. Synthesis of oxynitride glasses

Stoichiometric lithium disilicate ($Li_2Si_2O_5$) glasses were prepared with the addition of 0, 1.5, 3.0, 4.5, and 6.0 at.% N/(N+O) by the melt-quenching technique in a glove box under N_2 atmosphere. 50 g batches were prepared using high-purity-grade chemicals: Li_2CO_3 (99%, ACS reagent, Aldrich), quartz, SiO_2 (99%, ACS reagent, Merck), and Si_3N_4 (99%, Merck). The reagents were thoroughly mixed and melted at 1300°C for 1 h in molybdenum crucibles because

of their high melting temperature (2600°C) and of the absence of oxidation at 1300°C under pure nitrogen atmosphere. In addition, these crucibles are perfectly adapted to melting of silicates or phosphates glasses by means of a high frequency furnace. The glass melts were cast onto a molybdenum plate inside a glove box under N_2 atmosphere. Annealing was performed well below the glass transition temperature (T_g - 50°C) for 2 h to reduce the internal stresses without inducing significant crystal nucleation. The nitrogen content was determined using a LECO analyzer. No significant difference was found between the nominal and experimental values.

2.2. Density and mechanical properties

The density was measured using Archimedes' method in an alcoholic buoyant medium with an error of ±0.01 $g \cdot cm^{-3}$. Vickers microhardness was measured using a Vickers hardness tester (Equilam) under 50 MPa. The accuracy of the measured Vickers hardness was estimated to be within ±100 MPa. The Young's modulus was measured by the ultrasonic velocity technique. This technique is based on time-of-flight measurements using the pulse-echo technique and has an accuracy of ±2 GPa. The measured values of the above mentioned parameters are listed in Table 1.

2.3. XRD experiments and Rietveld refinement analysis

To identify the predominant crystalline phases after crystallization of the synthesized lithium silicate oxynitride glasses, vitreous samples were heated up to 800°C at a heating rate of $10°C \cdot min^{-1}$ and then slowly cooled down to room temperature by turning off the furnace. The treated samples were mounted in a rotating holder with a 27-mm-diameter ring. XRD experiments were performed on the Panalytical X'Pert Pro diffractometer with a Cu K_α anode

tube operating at 40 kV/40 mA; the detector used was the X'Celerator, using real-time multiple strip (RTMS) position-sensitive detection technology, which enables faster data collection than a conventional point detector. The scans were performed from 5° to 120° (2θ) with a step size of 0.026° (2θ) and counting times of 397 s per step in order to increase the number of data for Rietveld refinement. In addition, accuracy is better at high angles and important information about background is given at low angles, especially when a residual glassy phase is present. The range should always the widest possible, compatible with the instrument and collection time (no need to waste time if no reliable information is coming from a certain range). Pattern analysis was performed using the X'Pert HighScore Plus software (Panalytical). Structural data were selected after phase identification and were acquired from the inorganic crystal structure database (ICSD). The patterns were refined by the Rietveld method. The refined parameters were the zero shift, background coefficients, cell parameters, peak profiles, and phase fractions. This Rietveld quantitative analysis (RQA) compares the complete measured diffractogram with calculated diffractograms of all phases based on their structural data and minimizes the sum of the weighted squares of the deviations between the observed and theoretical intensities of the diffractogram. The analysis of a wide pattern minimizes the inaccuracies arising from systematic errors within the raw data, caused by, as examples, peak overlap or sample broadening. However, the crystal structures of all crystalline phases must be known in order to calculate the powder pattern.

The quantification of an amorphous phase is a step forward in the use of RQA. Analysis of amorphous phases in crystalline samples by adding a suitable internal standard have been reported [39]. Mixtures with a weighted amount of a well crystallized standard, in our case Y2O3, have been prepared with the investigated materials. Then mixtures have been analyzed by

powder diffraction and Rietveld phase analysis. If a sample has an amorphous phase, the crystalline phases will have smaller Rietveld refined weight ratios than those calculated from the weight mixtures. In the same way, the standard phase will be overestimated. The procedure relates the amorphous phase content to the small overestimation of the crystalline standard in the Rietveld refinement. It has been stated [40] that a proper phase analysis should allow the measurement of phase contents with an accuracy close to 2%.

2.4. Crystal growth measurements

Experimental crystal growth rates (U) were obtained by subjecting vitreous samples of dimensions 2.0 mm × 2.0 mm × 1.5 mm to isothermal treatments. All experiments were performed in a vertical furnace, and the temperature was monitored using a single appropriately calibrated (±1°C) K-type thermocouple. After the thermal treatments, the samples were polished and the polished face was attacked by an acid solution containing 0.2 HCl/0.6 HF (vol%) for 10 s. The formed crystals were observed in a Neophot Carl Zeiss Jena optical microscope using a 50X objective. The radii of the largest crystals were measured and plotted as a function of time. The crystal growth rates were obtained from the slopes of $dR/dt = U$.

2.5. DSC Analysis

Nonisothermal crystallization kinetics was determined in terms of the Avrami index and the activation energy for crystallization. For this purpose, DSC experiments were performed in a Netzsch DSC 404 apparatus. All experiments were performed using platinum crucibles under air atmosphere. Small vitreous samples weighing approximately 15 mg were subjected to different heating rates (ϕ = 10, 15, 20, and 25°C·min^{-1}) from 30°C until appearance of the crystallization

peak. The Ozawa method [41, 42] was employed to calculate the Avrami index n by the following equation:

$$-n = \left.\frac{\ln\left(-\ln\left(1-x\right)\right)}{\ln\phi}\right|_T \quad (1)$$

where x is the crystallized volume fraction obtained by area integration of the crystallization peak temperatures in the DSC experiments.

The activation energy for crystallization was calculated using the Ozawa method [43] by the following equation:

$$\ln\phi = \frac{E_C}{RT_P} + C\,, \quad (2)$$

where T_P is the crystallization peak temperature, R is the universal gas constant, and C is an empirical constant.

3. Results

The studied glasses changed from transparent colorless to deep gray with increasing nitrogen content. They were carefully observed under an optical microscope. They were free from bubbles, crystals, and striae after being annealed at a temperature below the glass transition temperature (T_g - 50°C) for 2 h. Table 1 presents the effects of the nitrogen content on the glass transition temperature (T_g) and crystallization peak temperature (T_P) (at 10°C·min^{-1}), densities, Vickers microhardness, and Young's modulus. The T_g values of the base glass (N0) did not show a significant difference (±3°C) from those obtained for previously studied glasses having the same nominal composition and melting conditions [44-46]. The same behavior was observed for the mechanical properties, such as the Vickers microhardness and Young's modulus [47,48].

It is evident that the addition of nitrogen to the $Li_2Si_2O_5$ glass also had a remarkable influence on all its properties listed in Table 1. For example, the T_g values changed by more than 50°C upon incorporation of nitrogen. The same behavior was observed for T_P (crystallization). In the case of T_g, this behavior can be explained by an increase in the network connectivity as a result of substitution of oxygen by nitrogen. The shift in T_P to higher values with an increase in nitrogen content can be explained by the appearance of the crystalline phase of lithium metasilicate ($Li_2Si_2O_3$), as shown in Fig. 1, which depletes the Li content of the residual vitreous matrix and increases its viscosity. A similar shift in T_p and an increased viscosity were observed when 3 mol% ZrO_2 was added to a $Li_2Si_2O_5$ glass [49, 50].

Table 1

Glass sample names, nitrogen contents, and respective glass transition temperatures (T_g), crystallization peak temperatures (T_p), densities (d), Vickers microhardness (H_v), and Young's moduli (E) of nitrited lithium disilicate ($Li_2Si_2O_5$) glasses.

Glass sample	at.% N/(N+O)	T_g (°C) (±3)	T_P (°C) (±3)	d (g·cm^{-3}) (±0.01)	H_v (MPa) (±100)	E (GPa) (±2)
N0	0	457	655	2.34	5222	80
N1.5	1.5	478	673	2.35	5612	81
N3	3	486	688	2.37	6230	86
N4.5	4.5	497	705	2.38	6343	87
N6	6	506	758	2.39	6448	88

3.1. ***Rietveld quantitative analysis (RQA)***

RQA relates the amorphous content, A (in wt%), to the overestimation of the internal standard in the Rietveld refinement, the following equation giving this value:

$$A = \frac{1 - \frac{W_s}{R_s}}{100 - W_s} \times 10^4 \qquad (4)$$

where W_S (in %) is the weighted concentration of the internal standard and R_s the Rietveld analyzed concentration of the standard.

The pure oxide glass crystallizes giving a single $Li_2Si_2O_5$ phase (JCPDS n°82-2396), it does not appear in this table. On the contrary, the presence of nitrogen enhances the crystallization of the Li_2SiO_3 phase (JCPDS n°83-1517). As can be seen, the more nitrogen content, the more Li_2SiO_3 phase. The weighted Y_2O_3 content (W_S = 30 wt% for each sample) doesn't match with the Rietveld analyzed concentration (R_S). For nitrogen contents up to 3%, the values of R_S are slightly lower than W_S, but for the others samples, this value increases and becomes overestimated. Nevertheless, in any cases, the Rietveld agreement factors (R_{wp}) are lower than 5% and the "Goodness of fit", namely the χ^2, does not exceed 7.5 for a theoretical attainable value of 1. It has been stated that R_{wp} and GOF values lower than 10% and 4, respectively, can be considered as quite good [51].

The samples with a nitrogen content lower than or equal to 3% are fully crystallized at 800°C. When the nitrogen content reaches 4.5% or more, Li_2SiO_3 becomes the main crystalline phase and an amorphous phase appears, thus the sample is assumed to be not fully crystallized. This residual glassy content (A%) is calculated by refining the diffraction patterns and assuming that $R_s = W_s$. (30%). The corrected weight contents are given in italics. We observe that the glassy

phase increases up to 30% while the $Li_2Si_2O_5$ content decreases down to 8% for the glass-ceramic the most enriched in nitrogen.

To gain a better understanding of this phenomenon, a schematic representation of the above-described crystallization process is shown in Fig. 1.

Table 2
Results of RQA (in wt%) in terms of Rietveld agreement factors (R_{wp} and *goodness of fit (GOF)*). Corrected values (numerals in italics) were obtained by fixing the Y_2O_3 content.

N/(N+O) (at.%)	$Li_2Si_2O_5$		Li_2SiO_3		Y_2O_3 (R_S)		*A*	R_{wp} (%)	*GOF*
	as deter.	*corr.*	*as deter.*	*corr.*	*as deter.*	*corr.*			
1.5	64.8	*63.4*	6.7	*6.6*	28.5	*30*	*0*	4.63	7.5
3	62.7	*61.5*	8.7	*8.5*	28.6	*30*	*0*	4.03	5.58
4.5	24.5	*23.4*	44.1	*42.2*	31.4	*30*	*4.4*	3.36	3.88
6	11.8	*8.2*	44.9	*31.2*	43.3	*30*	*30.6*	2.97	3.07

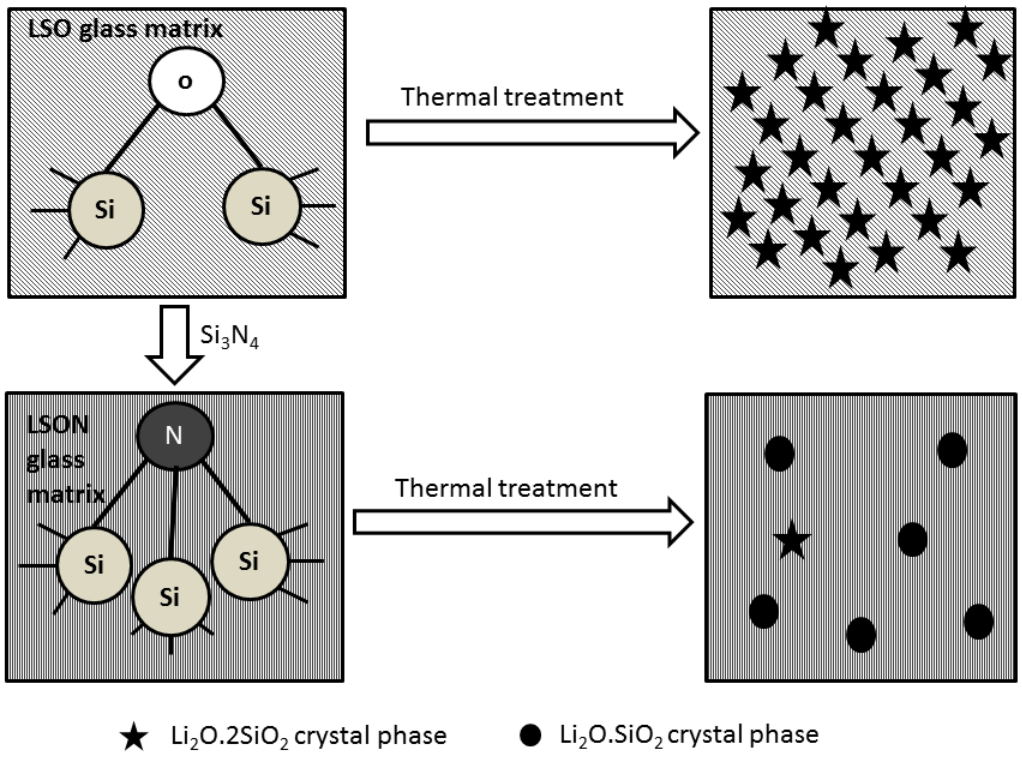

Fig. 1. -Schematic representation of Si-O and Si-N bonds and crystallization in lithium disilicate oxide (LSO) and lithium disilicate oxynitride (LSON) glasses.

3.2. Crystal growth measurements

The crystal growth rates (U) were measured by observing the crystals that grew after thermal treatments at 620, 650, and 690°C for different times under an optical microscope. Figure 2 shows optical microscopy (OM) images recorded in the reflected-light mode from the cross section of the glasses N1.5, N3, N4.5, and N6 that were treated at 620°C for 50 min. From these micrographs, it is evident that for all glasses, crystal growth was predominant in the sample interiors. The crystal morphology in the stoichiometric (N-free) lithium disilicate glass [45,48,52], i.e., ellipsoidal morphology, was corroborated for the N4.5, and N6 glasses, whereas a needle-like morphology was predominant in the N3 glass. Under any given thermal treatment,

the degree of crystallization decreased with an increase in nitrogen content. The glass N1.5 shows a significant degree of overall crystallization throughout the samples, whereas the other glasses exhibited a significant fraction of a residual glassy phase. Thieme and Russel [46] found that the $Li_2Si_2O_5$ and Li_2SiO_3 crystalline phases in ZrO_2-doped lithium disilicate glass had ellipsoidal and spherical crystal morphologies, respectively. In the present work, the Rietveld refinement analysis (Table 2) confirmed the existence of the $Li_2Si_2O_3$ crystalline phase and a decrease in the $Li_2Si_2O_5/Li_2Si_2O_3$ ratio.

The crystal growth rates were calculated from the time dependence of the radius (R) of the largest crystals observed on the cross sections, i.e., as $U = dR/dt$. In all cases (ellipsoidal and needle-like morphologies), the R values corresponded to the length of the major axis of the crystals. Figure 3 shows a plot of R as a function of time for the N3, N4.5, and N6 glasses heat-treated at 620°C for different times. The plot reveals a linear behavior. Moreover, it is clear that the crystal sizes decrease with increasing nitrogen content.

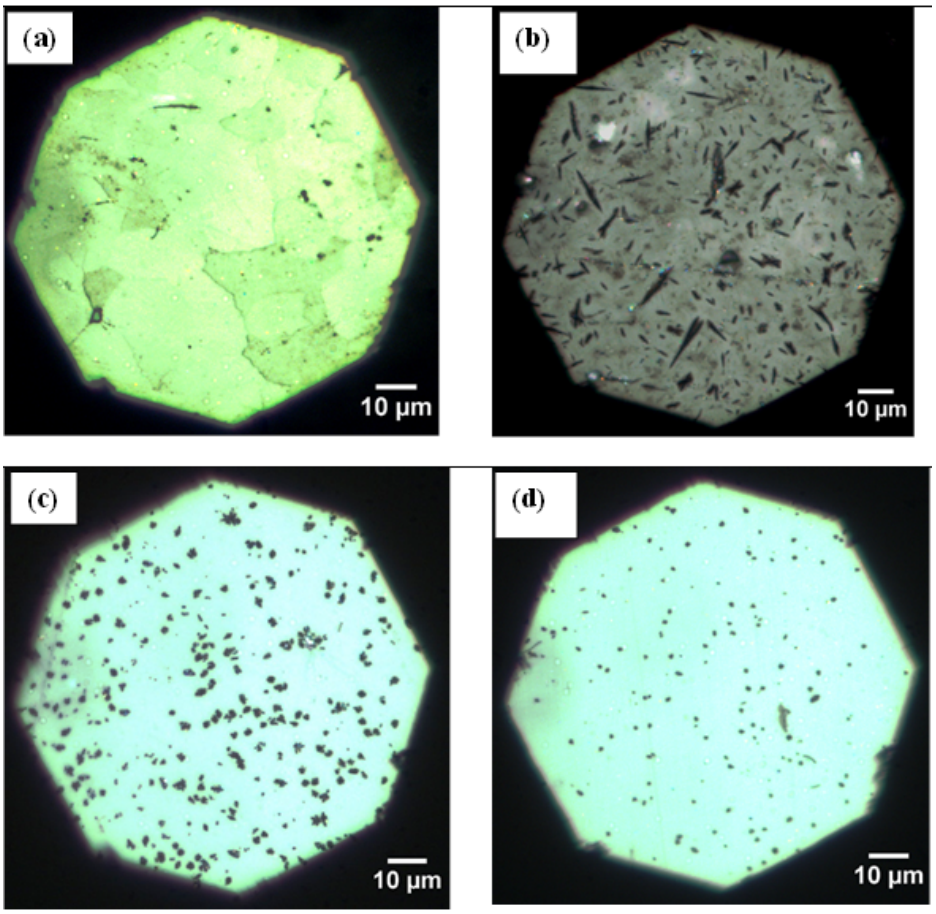

Fig. 2. -Optical microscopy images (50X objective) of (a) N1.5, (b) N3.0, (c) N4.5, and (d) N6 glasses heat-treated at 620°C for 50 min.

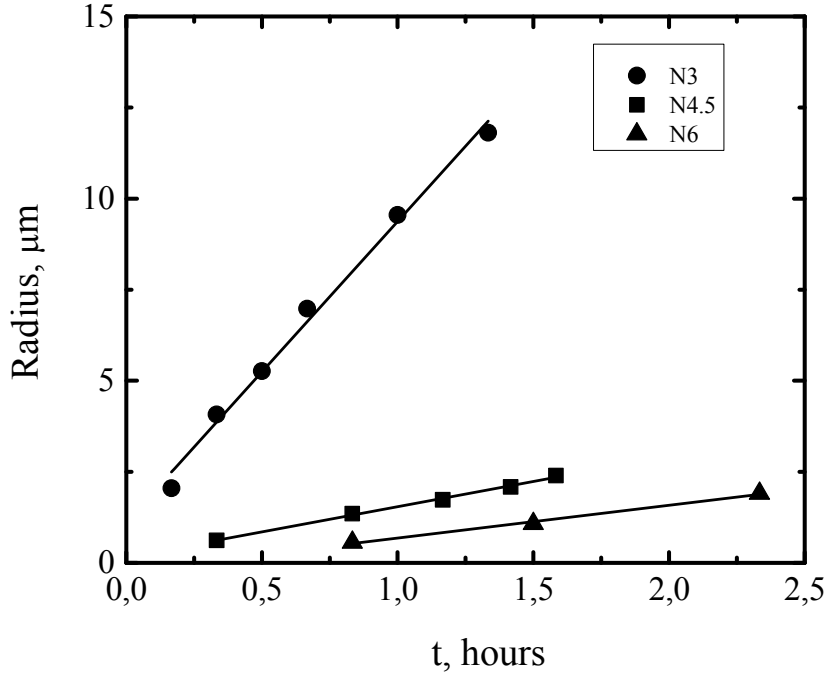

Fig. 3. -Crystal radius (*R*) as a function of time for N3, N4.5, and N6 glasses heat-treated at 620°C.

Figure 4 shows the temperature dependence of the crystal growth rates (*U*) for all the studied glass compositions at temperatures of 620, 650, and 690°C. The *U* values were calculated from the slopes of the plot of the time dependence of the radius (*R* versus *t*) illustrated in Fig. 3. As expected, the crystal growth rates increased with increasing temperature. It is noticeable from Fig. 4 that the crystal growth rates decreased significantly with increasing nitrogen content. For the N6 glass, temperature had a rather weak effect on the crystal growth rate. The crystal growth rates for all the glasses are summarized in Table 3.

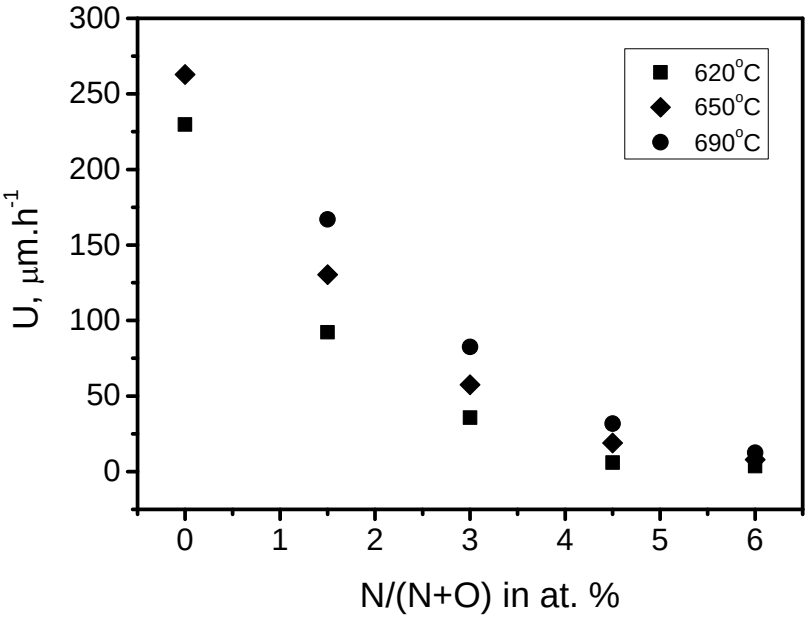

Fig. 4. -Crystal growth rate as a function of nitrogen content at 620, 650, and 690°C.

Table 3

Measured crystal growth rates (μm/h) for N0, N1, N3, N4.5, and N6 glasses.

T, °C / Glass	620	650	690
N0	2.304×10^2	2.628×10^2	
N1.5	1.3032×10^2	1.6704×10^2	1.98×10^2
N3	5.76×10	6.948×10	8.244×10
N4.5	7.92	1.908×10	3.1716×10
N6	3.6	6.012	1.008×10

3.3. Nonisothermal crystallization kinetics

The nonisothermal crystallization kinetics was characterized by DSC in terms of the Avrami index (n) and the effective activation energy for crystallization (E_c). DSC experiments were performed using monolithic pieces of glass (15 ± 0.1 mg), which were heated at different

heating rates (ϕ = 10, 15, 20, and 25°C·min^{-1}) from room temperature until appearance of the crystallization peak. As an example, Fig. 5 shows the DSC curves obtained for the N3 glass for different heating rates. The crystallization peak temperature and the peak height (δT_P) shifted to higher values with an increase in the heating rate. The same behavior was observed for all studied glasses.

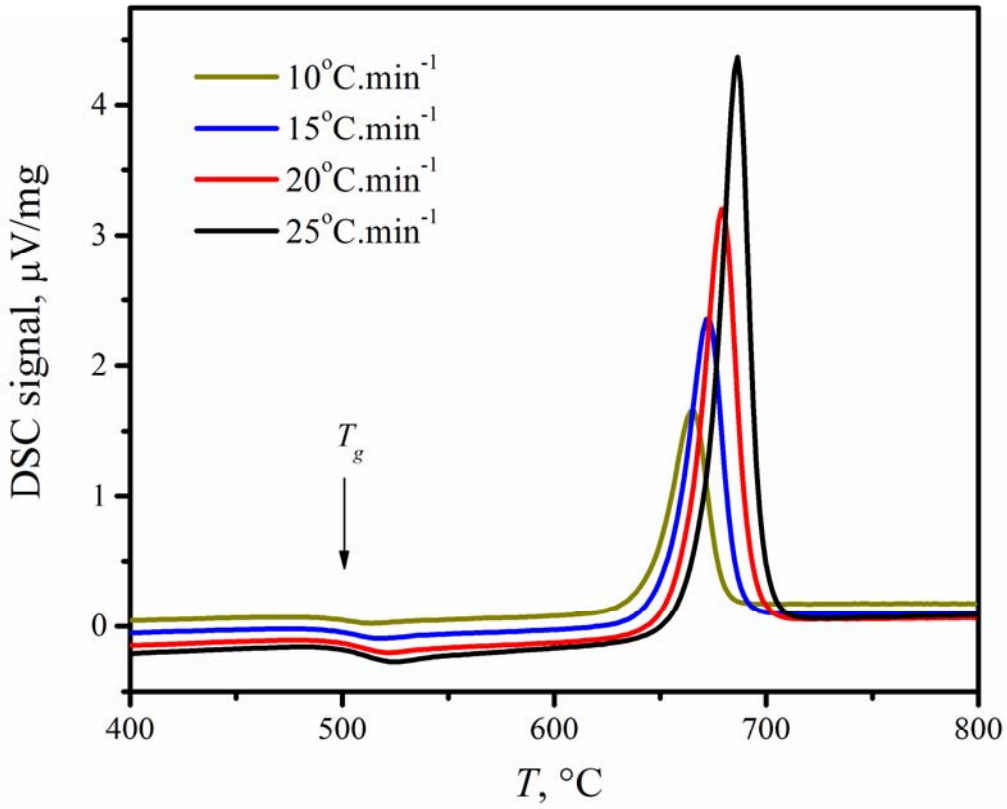

Fig. 5. -DSC curves obtained from bulk samples of N3 glass heated at different heating rates (ϕ = 10, 15, 20, and 25°C·min^{-1}).

The mathematical procedure to obtain n has been demonstrated in previous studies [53,54]. Figure 6 shows the plot of ln(-ln(1 - x)) versus ln(ϕ) (Eq. (1)) for the N3 glass. A linear

behavior was observed and the Avrami indexes were calculated from the slopes. The same procedure was performed for the N0, N1.5, N4.5, and N6 glasses (not shown here); the nitrogen content dependence of the Avrami index is plotted in Fig. 7. It is evident that the Avrami index increases with increasing nitrogen content, from approximately 2.6 to 4. In all cases, the Avrami index indicates that internal crystallization is predominant (over surface crystallization), which is in agreement with the micrographs in Fig. 2.

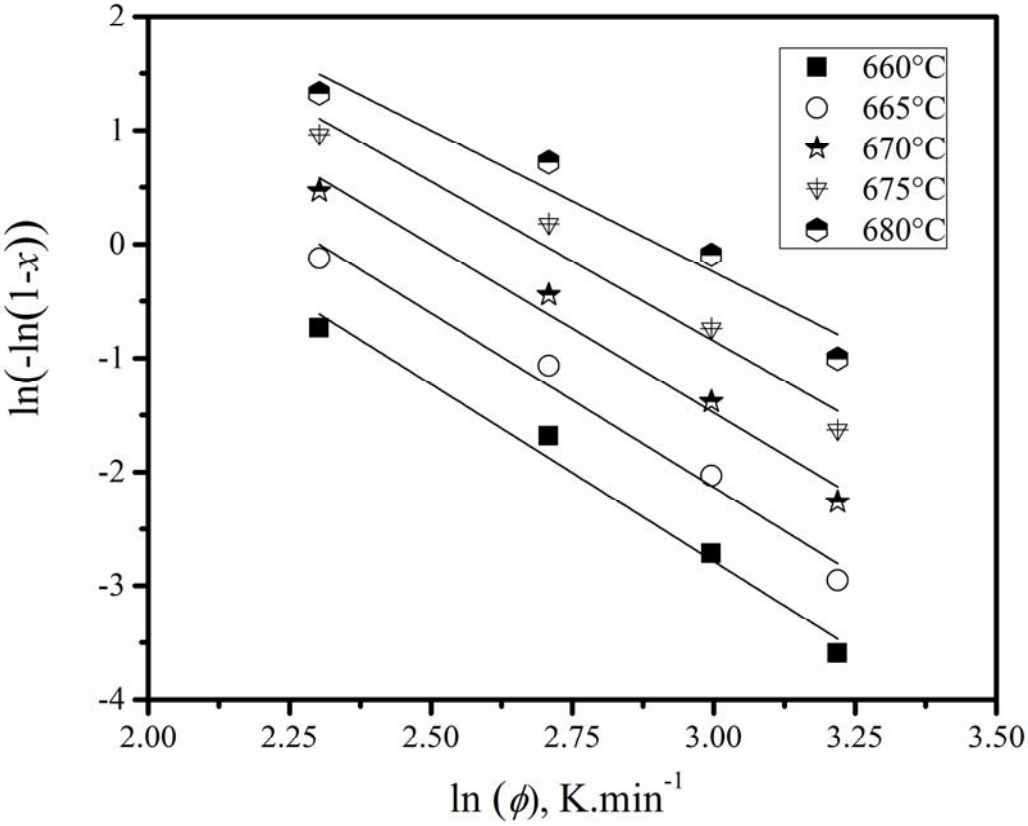

Fig. 6. -Plot of ln(-ln(1 - x)) versus ln(ϕ) for N3 glass.

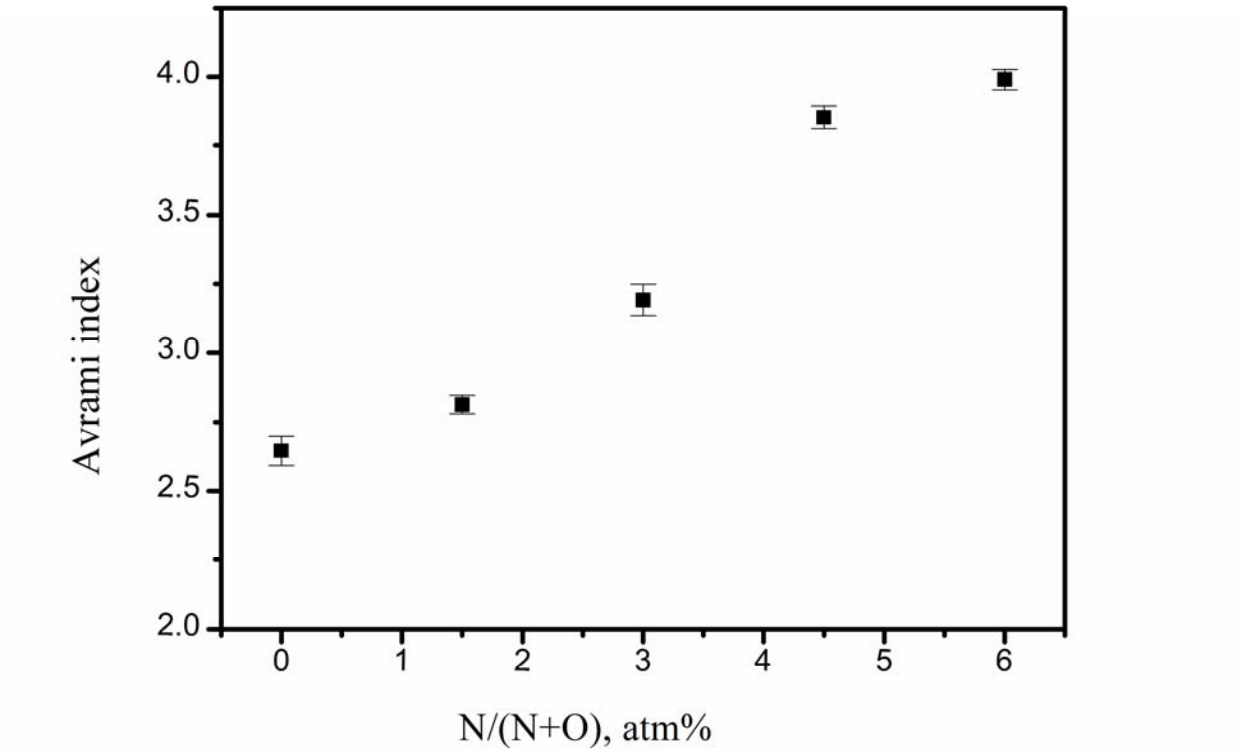

Fig. 7. -Dependence of Avrami index calculated from Eq. (1) on nitrogen content.

The fact that the *n* values for the N0, N1.5, N3, N4.5, and N6 glasses are different than 1, indicates volume crystallization. Therefore, the activation energy for crystallization cannot be calculated using the well-known Kissinger equation, which was derived for unidimensional growth [55]. In view of this fact, we used Ozawa's equation, Eq. (2), to estimate the E_c values [43]. Figure 8 shows the plot of $\ln(\phi)$ as a function of $10^3/T_P$ (where ϕ and T_P are the heating rate and crystallization peak temperature, respectively). The activation energy was determined from the slopes of the fitted lines, as shown in Fig. 9. Here, we consider that the pre-exponential term *C*, included in Eq. (2), is invariant relative to the exponential term for all the glasses. The activation energy corresponds to the growth of crystals, and it increases from 171 to 360 $kJ \cdot mol^{-1}$

with an increase in nitrogen content up to 6 at.% N/(N+O). Figure 8 shows the obtained Ozawa plots for the studied lithium disilicate oxynitride glasses.

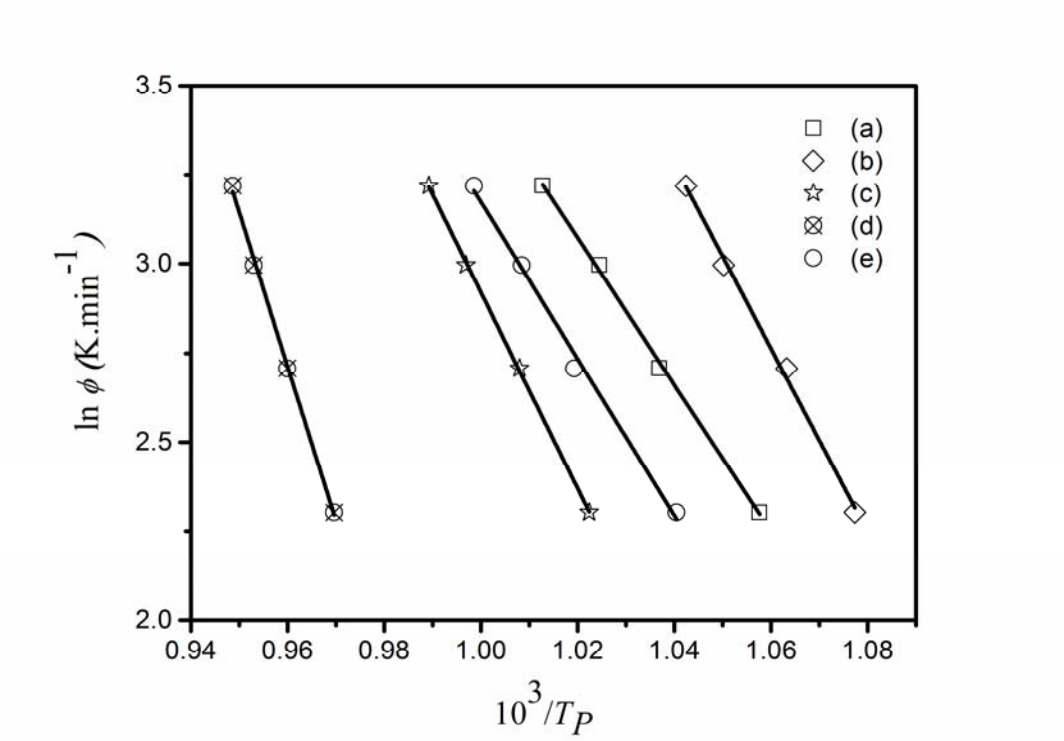

Fig. 8. -Ozawa plots for nitrited lithium disilicate glasses (a) N1.5, (b) N3, (c) N4.5, (d) N6, and (e) N0, obtained using Ozawa's equation.

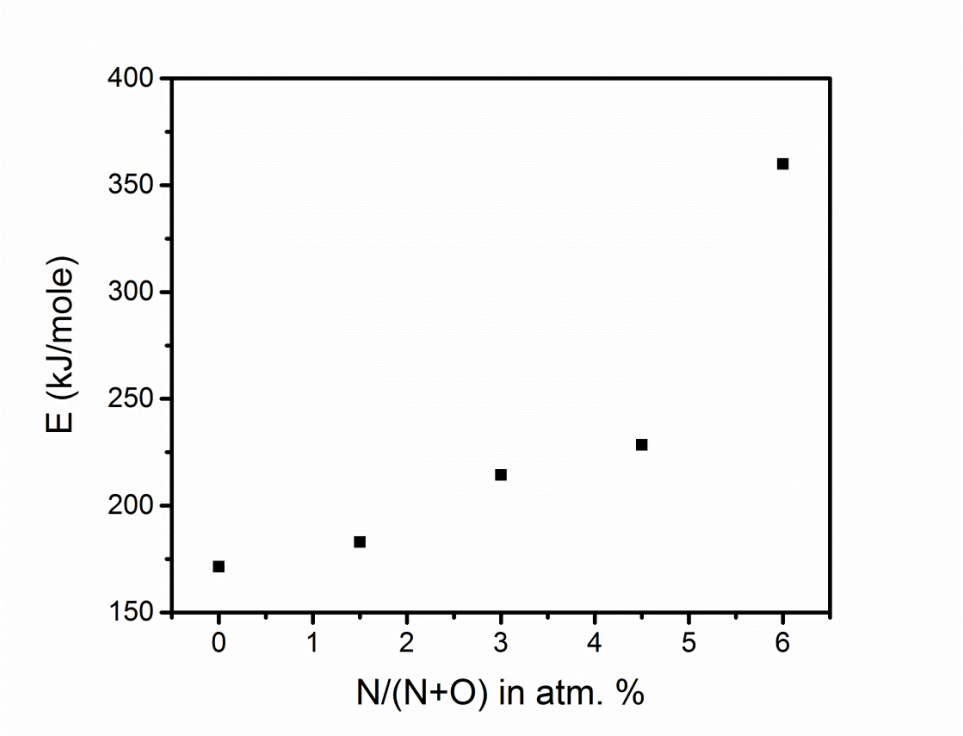

Fig. 9. -Activation energies for oxynitride glasses with different nitrogen contents.

4. Discussion

It is known that incorporation of nitrogen into any oxide glass network affects the glass properties considerably [23-32]. Most properties change in the direction that is expected from the increase in the connectivity of the glass network. The density and some mechanical properties, such as the Young's modulus and shear modulus, increase because of the increased network connectivity. This increase in the degree of network cross-linking, along with the more covalent nature of the nitrogen–modifier cation bonding, causes the glass network to contract and rigidify. The strength of the Si-O bond (~452 $kJ \cdot mol^{-1}$) is higher than that of the Si-N bond (355 $kJ \cdot mol^{-1}$), and hence, increase in the local bond density results in a net increase in the local bond energy and the elastic moduli. To explore how and why hardness varies with the degree of nitridation, a

previous study developed a topological model of oxynitride glass hardness by using temperature-dependent constraint theory [29]. According to this linear model, the hardness increase is the result of the increase in the number of both bond-bending and bond-angular constraints. This model is applicable for several alkaline-earth aluminosilicate glasses.

The Rietveld refinement analysis revealed that introduction of nitrogen into the glass structure and subsequent heat treatment of the considered glass samples caused a phase conversion from lithium disilicate to lithium metasilicate. This is the most interesting finding of this research. The fact that silicon could not enter into the crystalline phase (to form the disilicate) is probably a result of its strong bonding with nitrogen, which has three-coordination (Fig. 1). The Rietveld refinement analysis did not provide any indication of incorporation of nitrogen into the lithium disilicate or lithium metasilicate crystals, which indicates that the nitrogen remained in the residual glassy phase, which was silica-enriched because most lithium was essentially consumed by the two crystalline phases. Evidence of such (residual) silicon oxynitride glass was provided in a previous study [56]. In this previous study, synthesis of silicon oxynitride glasses was achieved through nitridation, at temperatures of up to 1300°C, of a commercial colloidal silica (Cab-O-Sil (EH-5 S-17, 99.5%, 380 $m^2 \cdot g^{-1}$)). Glasses with a maximum nitrogen content of up to 24.5% (as determined by the N/(N+O) atomic ratio) were obtained with a T_g of around 1195°C (at 15°C·min^{-1}). XRD confirmed that all nitrided samples of Cab-O-Sil were amorphous. Samples with N/(N+O) values in the range of 24.5%–43.6% were partially crystallized and they showed both □- and □-Si_3N_4 as the crystalline phases.

As revealed by the Rietveld refinement analysis in the present study, all lithium ions are consumed by the oxide crystalline phases ($Li_2Si_2O_5$ and Li_2SiO_3), as a result of which nitrogen should mostly be in the residual glassy phase. Thus, this assumption permits calculation of the

maximum nitrogen content of the residual silica phase. The general formula for oxynitride glasses is $Li_2Si_2O_{5-x}N_{2x/3}$. Thus, the nitrogen content is given by

$$\frac{N}{(N+O)} = \frac{\frac{2x}{3}}{\frac{2x}{3}+5-x}$$

For a maximum nitrogen content of about 6 at.%, the x value is 0.437 .

Nitrided silica should have the formula $SiO_{2-x}N_{2x/3}$. Substitution of the calculated value of x into this formula causes it to be modified to $SiO_{1.563}N_{0.291}$ and $\frac{N}{(N+O)} = 15.7\%$.

This nitrogen content corroborates the above hypothesis of the nitrogen being in the residual glass phase. As a consequence, the viscosity of this residual glass becomes higher than that of the parent glass, and the ability of the silica-rich oxynitride glass to crystallize is then modified.

The thermal properties of oxynitride glasses, e.g., T_g and T_P, which depend on the structure and nature of bonds, are then clearly affected. These two temperatures increase with increasing nitrogen content as the rigidity of the glasses improves; this is confirmed by the increase in the different elastic moduli, which are generally considered as indicators of the glass network rigidity.

The DSC thermogram for the N3 glass in Fig. 5 shows the shift of the crystallization peak temperature to a higher value with an increase in the heating rate. Such a shift of the crystallization peak temperature implies the presence of a high concentration of nuclei at low heating rates because of the longer time for nucleation. Therefore, crystallization occurs in a shorter period of time at higher heating rates, and the peak is narrower and it should be more intense than those obtained at lower heating rates.

The Avrami index (n) is a useful parameter for identifying the predominant crystallization mechanisms. An n value of ~3 suggests bulk or three-dimensional crystal growth, whereas values close to 1 suggest surface nucleation and growth [57]. In this study, we found that the Avrami index of the glasses varied in the range of 2.6-4 and gradually increased with increasing nitrogen content of the glass. This behavior has already been observed for LiSiAlON glasses [37-38], whose Li/Si atomic ratio is 1. These glasses can be described by the formula $Li_2Si_2Al_{0.33}O_{5.5-x}N_{2x/3}$. Their nonisothermal DTA studies revealed that the Avrami index was about 1.8 for the oxide glass and about 3.1 for an oxynitride glass with N/(N+O) of about 3%.

The values of n suggest that crystallization occurs in the sample interiors and that the growth is three-dimensional. The activation energies for all the glasses were calculated using Ozawa's model. The activation energies increased with increasing nitrogen content because of an increase in the connectivity of the glass network, as described earlier. Introduction of nitrogen into the glass made the glass network more rigid, caused the viscosity to increase, and resulted in a larger amount of energy being required for the mobility of the species to form crystals. These activation energies are comparable to those obtained for the LiSiAlON glasses, i.e., 182 and 232 $kJ \cdot mol^{-1}$ for the oxide and oxynitride glasses, respectively [37-38]. These numerical values are rather similar and the increase in E_c with nitrogen incorporation is quite the same when the N/(N+O) ratios are similar.

Although it has been reported that oxynitride glasses can be converted to fine-textured glass-ceramics [58], the precise mechanism of nucleation remains uncertain. A reasonable possibility to be considered is that the incorporation of nitrogen may promote phase separation, which might induce precipitation of a large number of nuclei. Another hypothesis could be associated with the fact that oxynitride glasses are usually gray in color. According to a previous

study on YSiAlON glasses [59], this color may be attributed to the presence of a small amount of fine metallic silicon produced from the decomposition of silicon nitride. Energy-dispersive X-ray spectroscopy (EDX) observations showed the presence of spherical particles with diameters of up to 50 μm consisting of Fe and Si, Fe being a significant impurity in most glasses. Thus, it was concluded that the metallic particles were undesirable because they reduce glass transparency and may act as unwanted nucleation sites. In our study, the amount of silicon particles (if they actually existed) was so small that they could not be detected by XRD. It should be noted that a previous study on LiSiON glasses [60] revealed that in oxide glasses, the crystallization temperatures of powder specimens were about 100°C lower than those of bulk specimens, suggesting the occurrence of surface crystallization. In oxynitride glasses, the differences in the crystallization temperatures between the powder and the bulk specimens were smaller, suggesting that the effect of the surface on the crystallization of oxynitride glasses was small. In the above-cited study, the change in the nucleation mechanism between oxide and oxynitride glasses was substantiated by SEM [60].

Moreover, heat treatments performed at temperatures in the range of 670-925°C for different durations ranging between 1 and 24 h caused the crystalline phases to vary with the nitrogen content [60]. Li_2SiO_3 as well as $Li_2Si_2O_5$ precipitated, but the crystallization tendency of Li_2SiO_3 became more pronounced as the nitrogen content increased. However, owing to a Li/Si atomic ratio of about 0.85, cristobalite was also found in the oxynitride glasses. Moreover, no crystalline phase containing nitrogen was observed after the heat treatment at 925°C for 24 h. This behavior is corroborated by the Rietveld refinement analysis, which reveals that at higher nitrogen contents, lithium metasilicate is the predominant crystal phase after heat treatment at temperatures above T_g. The above phenomenon is schematically shown in Fig. 1.

Different factors limit the accuracy of the Rietveld method: particle statistics, preferred orientation, and microabsorption. It is generally acknowledged that for quantitative phase analysis, the peak intensities need to be measured to an accuracy of about ±1–2% [61]; the ability to achieve this is strongly influenced by the size of the crystallites and the number of diffracting crystallites in the sample. The effect of particle size statistics in a sample has been studied [62], and it has been revealed that diffraction by crystallites increases significantly when the particle size of the powder decreases.

The increases in the activation energy and the Avrami index with an increase in the nitrogen content to 6 at.% lead to an increase in the value of T_g by up to 50°C. This finding corroborates previous results, implying that the incorporation of nitrogen into the glass network increases the stability of the glass structure. The OM images of glasses containing different nitrogen contents, shown in Fig. 2, reveal that the shape and concentration of the crystals change significantly with the nitrogen content. The growth rate of the crystals decreases with an increase in the nitrogen content. This decrease in growth rates is caused by the introduction of nitrogen into the glass. This result also corroborates the theory that after nitrogen incorporation, the glass structure becomes more polymerized and viscous and hinders crystal growth. On the basis of the above discussion, it can be said that the nitrogen content affects the crystallization process of the glass. Moreover, at higher nitrogen contents, the percentage of lithium disilicate crystals decreases with a concurrent increase in the lithium metasilicate phase.

5. Summary and Conclusions

In this paper, we report on the crystallization pathways and kinetics of oxynitride glasses having a lithium disilicate composition. We studied the effects of nitrogen content on different

properties of the glasses. In these mixed ionic glasses, oxygen was partially substituted by nitrogen (up to 6 at.% N/(N+O)), and the glass density, microhardness and Young's modulus increased with increasing nitrogen content. Thermal properties such as the glass transition temperature (T_g) and crystallization peak temperature (T_P) also increased with the introduction of nitrogen. Increases in the activation energy of crystallization and the Avrami index with an increase in the nitrogen content were also observed. However, the growth rate of crystals decreased with an increase in the nitrogen content.

Most of these changes in properties were expected and can be explained by the change in the glass network upon the partial substitution of oxygen by nitrogen. Nitrogen has a higher coordination number than oxygen, which enhances the connectivity of the glass network as well as the atomic packing density.

Upon thermal treatment at high temperatures after the addition of nitrogen, lithium metasilicate formed gradually at the expense of the (expected) equilibrium lithium disilicate phase. This is the most fascinating and unexpected finding of this research. The improved mechanical properties and unusual crystallization behavior of these oxynitride glass-ceramics may renew interest in them and thus warrant further research.

Acknowledgements

The authors are grateful to the São Paulo Research Foundation, Brazil (FAPESP, Grant Nos. #2013/09093-1 and 2013/07793-6), for the financial support to this research project. The authors are also thankful to Dr. Maziar Montazerian for his critical comments.

References

[1] M. Montazerian, S.P. Singh, E.D. Zanotto, An analysis of glass-ceramic research, Am. Ceram. Soc. Bull. 94 (4) (2015) 30-35.

[2] T. Komatsu, Design and control of crystallization in oxide glasses, J. Non-Cryst. Solids 428 (2015) 156-175.
[3] L.L. Hench, The future of bioactive ceramics, J. Mater. Sci. Mater. Med. 26 (2015) 86.
[4] J.C. Mauro, E.D. Zanotto, Two centuries of glass research: Historical trends, current status, and grand challenges for the future, Int. J. Appl. Glas. Sci. 5 (2014) 313-327.
[5] P. Goharian, A. Nemati, M. Shabanian, A. Afshar, Properties, crystallization mechanism and microstructure of lithium disilicate glass-ceramic, J. Non-Cryst. Solids 356 (2010) 208-214.
[6] O. Kanert, R. Küchler, P.C. Soares, H. Jain, Nearly constant loss behavior of lithium disilicate during devitrification, J. Non-Cryst. Solids 307-310 (2002) 1031-1038.
[7] A. Gaddam, H.R. Fernandes, D.U. Tulyaganov, M.J. Pascual, J.M.F. Ferreira, Role of manganese on the structure, crystallization and sintering of non-stoichiometric lithium disilicate glasses, RSC Adv. 4 (2014) 13581-13592.
[8] Z.E. Biskri, H. Rached, M. Bouchear, D. Rached, Computational study of structural, elastic and electronic properties of lithium disilicate ($Li_2Si_2O_5$) glass-ceramic, J. Mech. Behav. Biomed. Mater. 32 (2014) 345-350.
[9] F. Wang, Z. Chai, Z. Deng, J. Gao, H. Wang, J. Chen, Effect of heat-pressing temperature and holding time on the microstructure and flexural strength of lithium disilicate glass-ceramics, PLoS ONE 10 (5) (2015) 1-10.
[10] W. Lien, H.W. Roberts, J.A. Platt, K.S. Vandewalle, T.J. Hill, T.-M.G. Chu, Microstructural evolution and physical behavior of a lithium disilicate glass-ceramic, Dent. Mater. 31 (2015) 928-940.
[11] X.-F. Song, H.-T. Ren, L. Yin, Machinability of lithium disilicate glass ceramic in in vitro dental diamond bur adjusting process, J. Mech. Behav. Biomed. Mater. 53 (2016) 78-92.
[12] F.H. ElBatal, M.A. Ouis, A.M. Abdelghany, N.A. Ghoneim, Structural and optical correlation of gamma-irradiated 3d transition metals-doped lithium disilicate glasses, Silicon 7 (2015) 409-417.
[13] F.C. Serbena, I. Mathias, C.E. Foerster, E.D. Zanotto, Crystallization toughening of a model glass-ceramic, Acta Mater. 86 (2015) 216-228.
[14] J. Du, L.R. Corrales, Structure, dynamics, and electronic properties of lithium disilicate melt and glass, J. Chem. Phys. 125 (2006) 114702.
[15] S. Huang, Z. Huang, W. Gao, P. Cao, Structural response of lithium disilicate in glass crystallization, Cryst. Growth Des. 14 (2014) 5144-5151.
[16] C. Schröder, M.D.O.C. Villas-Boas, F.C. Serbena, E.D. Zanotto, H. Eckert, Monitoring crystallization in lithium silicate glass-ceramics using $^{7}Li \rightarrow {}^{29}Si$ cross-polarization NMR, J. Non-Cryst. Solids 405 (2014) 163-169.
[17] K. Thieme, C. Rüssel, Nucleation and growth kinetics and phase analysis in zirconia-containing lithium disilicate glass, J. Mater. Sci. 50 (2015) 1488-1499.
[18] S. Krüger, J. Deubener, Stochastic nature of the liquid-to-crystal heterogeneous nucleation of supercooled lithium disilicate liquid, J. Non-Cryst. Solids 388 (2014) 6-9.
[19] E.D. Zanotto, M.L.G. Leite, The nucleation mechanism of lithium dissilicate glass revisited,

J. Non-Cryst. Solids 202 (1996) 145-152.
[20] J. Deubener, R. Brückner, M. Sternitzke, Induction time analysis of nucleation and crystal growth in di- and metasilicate glasses, J. Non-Cryst. Solids 163 (1993) 1-12.
[21] D.J.M. Burkhard, N.V. Russell, Nucleation characteristics of lithium disilicate at pressures to 0.5 GPa, J. Non-Cryst. Solids 171 (1994) 236-242.
[22] S. Huang, Z. Huang, W. Gao, P. Cao, Trace phase formation, crystallization kinetics and crystallographic evolution of a lithium disilicate glass probed by synchrotron XRD technique, Sci. Rep. 5 (2015) 9159-1-5.
[23] S. Ali, B. Jonson, M.J. Pomeroy, S. Hampshire, Issues associated with the development of transparent oxynitride glasses, Ceram. Int. 41 (2015) 3345-3354.
[24] P.F. Becher, S. Hampshire, M.J. Pomeroy, M.J. Hoffmann, M.J. Lance, R.L. Satet, An overview of the structure and properties of silicon-based oxynitride glasses, Int. J. Appl. Glas. Sci. 2 (2011) 63-83.
[25] T. Das, Oxynitride glasses - An overview, Bull. Mater. Sci. 23 (2000) 499-507.
[26] S. Hampshire, Oxynitride glasses, their properties and crystallisation - A review, J. Non-Cryst. Solids 316 (2003) 64-73.
[27] J. Rocherullé, M. Matecki, Y. Delugeard, Heat capacity measurements of Mg-Y-Si-Al-O- N glasses, J. Non-Cryst. Solids 238 (1998) 51-56.
[28] J.M. Reau, H. Kahnt, J. Rocherullé, P. Verdier, Y. Laurent, The influence of nitrogen on the mobility of lithium in oxynitride glasses of the Li-Si-Al-O-N system, J. Non-Cryst. Solids 155 (1993) 185-188.
[29] G.L. Paraschiv, S. Gomez, J.C. Mauro, L. Wondraczek, Y. Yue, M.M. Smedskjaer, Hardness of oxynitride glasses: Topological origin, J. Phys. Chem. B 119 (2015) 4109-4115.
[30] S. Sakka, Structure, properties and application of oxynitride glasses, J. Non-Cryst. Solids 181 (1995) 215-224.
[31] Z. Luo, G. Qu, X. Chen, X. Liu, A. Lu, Effects of nitrogen and lanthanum on the preparation and properties of La-Ca-Si-Al-O-N oxynitride glasses, J. Non-Cryst. Solids 361 (2013) 17-25.
[32] Z. Luo, G. Han, A. Lu, Zn-Sr mixing in the Y-sialon glass: Formation, properties and ballistic resistance, J. Non-Cryst. Solids 421 (2015) 41-47.
[33] A. Le Sauze, R. Marchand, Chemically durable nitrided phosphate glasses resulting from nitrogen/oxygen substitution within PO_4 tetrahedra, J. Non-Cryst. Solids 264 (2000) 285-292.
[34] G.L. Paraschiv, F. Muñoz, L.R. Jensen, Y. Yue, M.M. Smedskjaer, Impact of nitridation of metaphosphate glasses on liquid fragility, J. Non-Cryst. Solids 441 (2016) 22-28.
[35] G. Qu, X. Hu, L. Cui, A. Lu, Synthesis, crystallization behavior and microstructure of oxynitride glass-ceramics with different modifier elements, Ceram. Int. 40 (2014) 4213-4218.
[36] J. Rocherullé, M. Matecki, B. Baron, P. Verdier, Y. Laurent, A devitrification study of Mg-Y-Si-A1-O-N glasses, J. Non-Cryst. Solids 211 (1997) 222-228.

[37] H. Héliès, J. Rocherullé, Kinetics of a las oxynitride glass crystallization, J. Mater. Sci. Lett. 21 (2002) 1921-1922.
[38] J. Rocherullé, T. Marchand, Nonisothermal devitrification study of an aluminosilicate glass matrix, Mater. Res. Bull. 35 (2000) 9-14.
[39] R. S. Winburn, S. L. Lerach, B. R. Jarabek, M. A. Wisdom, D. G. Grier, G.J. Mc Carthy, Quantitative XRD analysis of coal combustion by-products by the Rietveld method. Testing with standard mixtures, Adv. X-ray Anal. 42 (2000) 387- 396.
[40] A. G. De la Torre, M. A. G. Aranda, Accuracy in Rietveld quantitative phase analysis of Portland cements J. Appl. Cryst. 36 (2003) 1169-1176.
[41] T. Ozawa, Kinetics of non-isothermal crystallization, Polymer 12 (1971) 150-158.
[42] R. Wurth, M.J. Pascual, G.C. Mather, A. Pablos-Martín, F. Muñoz, A. Durán, G.J. Cuello, C. Rüssel, Crystallisation mechanism of a multicomponent lithium alumino-silicate glass, Mater. Chem. Phys. 134 (2012) 1001-1006.
[43] K. Biswas, A.D. Sontakke, S. Balaji, A.R. Molla, K. Annapurna, Crystallization kinetics and luminescence properties of a new low phonon Bi_2O_3-ZnO-GeO_2 glass, Phys. Chem. Glas. Eur. J. Glas. Sci. Technol. B 54 (2013) 206-215.
[44] A.M. Rodrigues, A.M.C. Costa, A.A. Cabral, Effect of simultaneous nucleation and crystal growth on DSC crystallization peaks of glasses, J. Am. Ceram. Soc. 95 (2012) 2885-2890.
[45] K. Thieme, C. Rüssel, Nucleation inhibitors—the effect of small concentrations of Al_2O_3, La_2O_3 or TiO_2 on nucleation and crystallization of lithium disilicate, J. Eur. Ceram. Soc. 34 (2014) 3969-3979.
[46] K. Thieme, C. Rüssel, Nucleation and growth kinetics and phase analysis in zirconia-containing lithium disilicate glass, J. Mater. Sci. 50 (2015) 1488-1499.
[47] S.K. Dubrovo, Y.A. Shmidt, Physicochemical properties of vitreous lithium silicates and aluminosilicates, Zh. Prikl. Khim. 32 (1959) 742-749.
[48] T. Zhao, Y. Qin, P. Zhang, B. Wang, J.-F. Yang, High-performance, reaction sintered lithium disilicate glass-ceramics, Ceram. Int. 40 (2014) 12449-12457.
[49] K. Matusita, S. Sakka, T. Maki, M. Tashiro, Study on the crystallization of glass by differential thermal analysis. Effect of added oxide on crystallization of Li_2O–SiO_2, J. Mater. Sci. 10 (1975) 94-100.
[50] C.C. Lin, P. Shen, H.M. Chang, Y.J. Yang, Composition dependent structure and elasticity of lithium silicate glasses: Effect of ZrO_2 additive and the combination of alkali silicate glasses, J. Eur. Ceram. Soc. 26 (2006) 3613-3620.
[51] B. H. Toby, R factors in Rietveld analysis: How good is good enough? Powder diffract. 21 (2006) 67-70
[52] V.M. Fokin, A.A. Cabral, R.M.C.V. Reis, M.L.F. Nascimento, E.D. Zanotto, Critical assessment of DTA–DSC methods for the study of nucleation kinetics in glasses, J. Non-Cryst. Solids 356 (2010) 358-367.
[53] A.M. Rodrigues, J.M.R. Mercury, V.S. Leal, A.A. Cabral, Isothermal and non-isothermal crystallization of a fresnoite glass, J. Non-Cryst. Solids 362 (2013) 114-119.

[54] A.R. Molla, A.M. Rodrigues, S.P. Singh, R.F. Lancelotti, E.D. Zanotto, A.C.M. Rodrigues, R. Dousti, A.S.S. de Camargo, C. J. Magon, I.D´A. Almeida Silva, Crystallization, mechanical and optical properties of transparent, nanocrystalline gahnite glass-ceramics, J. Am. Ceram. Soc. (2017) (in press).

[55] K. Matusita, S. Sakka, Kinetic study of crystallization of glass by differential thermal analysis-criterion on application of Kissinger plot, J. Non-Cryst. Solids 38-39 (1980) 741-746.

[56] F. Muñoz, D. Benne, L. Pascual, J. Rocherullé, R. Marchand, C. Rüssel, A. Durán, Silicon oxynitride glasses produced by ammonolysis from colloidal silica, J. Non-Cryst. Solids 345-346 (2004) 647-652.

[57] R.S. Soares, R.C.C. Monteiro, M.M.R.A. Lima, R.J.C. Silva, Crystallization of lithium disilicate-based multicomponent glasses–effect of silica/lithia ratio, Ceram. Int. 41 (2014) 1-8.

[58] W.K. Tredway, S.H. Risbud, Preparation and controlled crystallization of SiBaAlON oxynitride glasses, J. Non-Cryst. Solids 56 (1983) 135-140.

[59] D.R. Messier, E.J. Deguire, Thermal decomposition in the system YSiAION, J. Am. Ceram. Soc. 67 (1984) 602-605.

[60] H. Unuma, T. Kokubo, S. Sakka, Crystallization of LiSiON glasses, J. Mater. Sci. 23 (1988) 4399-4405.

[61] R.E. Dinnebier, S.J.L. Billige, in Powder diffraction, theory and practice, RSC Publishing, 2008, Cambridge, UK.

[62] D.K. Smith, Particle statistics and whole-pattern methods in quantitative x-ray powder diffraction analysis, Adv. X-ray Anal. 35 (1992) 1-15.